

Simulation of chlorine release in an industrial facility – FLUENT and HPAC model results

Thor Gjesdal, Jens William Bjerkelund and Audun Bjerke

Norwegian Defence Research Establishment (FFI)

31 October 2008

FFI-rapport 2008/01732

1048

P: ISBN 978-82-464-1533-8

E: ISBN 978-82-464-1534-5

Keywords

Klorutslipp

Spredning

Computational Fluid Dynamics (CFD)

FLUENT

Gaussisk puff-modellering

HPAC

Approved by

Monica Endregard

Project manager

Bjarne Haugstad

Director of Research

Jan Ivar Botnan

Director

English summary

We consider the release and dispersion of gaseous chlorine in an industrial facility. We have used a test case for which experimental reference data, upscaled from wind tunnel tests, are available. This test case has been simulated both with a complex CFD model (FLUENT) and with a simplified model (HPAC).

CFD modeling can reproduce the reference data fairly well, both with respect to the trajectory of the plume and to the concentration values. HPAC simulations can not take into account deflection of the plume by the momentum-driven release jet and plume-building interactions, and also give results in which the dilution of the plume appears to be more rapid than in the reference data.

Sammendrag

Vi diskuterer utslipp og spredning av klorgass i et industrianlegg. Vi har tatt utgangspunkt i et scenario hvor det finnes eksperimentelle referansedata som er oppskalert fra vindtunnelforsøk. Dette tilfellet har blitt simulert både med en kompleks CFD-modell (FLUENT) og en forenklet modell (HPAC).

CFD-modellering reproducerer referansedataene godt, både med hensyn på gasskyens utbredelse og konsentrasjonsverdier. HPAC-simuleringene kan ikke ta hensyn til avbøyning av det momentum-drevne utslippet. Disse resultatene viser også for rask uttynning av gasskyen sammenliknet med referansedata.

Contents

1	Introduction	7
2	Scenario description	8
3	FLUENT simulations	8
3.1	Geometry and grid	10
3.2	Turbulence model and boundary conditions	12
3.3	Simulations	12
3.4	Simulation results	12
3.4.1	Statistical analysis	13
3.4.2	Plume profiles	15
3.4.3	Horizontal downwind profiles	16
3.4.4	Horizontal cross-plume profiles	16
3.4.5	Vertical cross-plume profiles	19
4	HPAC model results	24
4.1	Simulation set-up	24
4.2	Simulation results	24
4.2.1	Downwind profiles	25
4.2.2	Cross-wind profiles	26
5	Conclusions	31

1 Introduction

Toxic Industrial Chemicals (TIC) can pose a potential hazard at facilities for production, processing, and storage or during transport. The most immediate hazard comes from accidental release. Malign use of such chemicals as a weapon through intentional release can, however, not be ruled out, especially in conflict or post-conflict zones that may have poor or non-existing infrastructure and derelict or abandoned production and storage facilities.

There exists a large number of modeling approaches to predict the consequences of the release of a potentially harmful substance to the atmosphere. Such models are important tools for the assessment of consequences, countermeasures, and emergency response and planning. A dispersion model comprises mathematical and physical description of a number of interdependent processes that constitute a complete release and dispersion event. Modeling can, largely, be divided into the description of three interdependent phases:

1. Source/release modeling.
2. Transport modeling.
3. Effects modeling.

Models of differing complexity can be developed by making different modeling assumptions and simplifications. Traditionally, relatively simple dispersion models have been used, but the increasing availability of computing power now enables the use of more complex models.

The development, application and validation of dispersion models go hand-in-hand. Even models that take into account a sophisticated description of the physical phenomena inherent in the dispersion processes are based on assumptions and simplifications that must be calibrated against realistic data. There is therefore a need for well-documented test cases and experimental reference data.

In this report we consider a scenario for which reference data are available. These data are taken from wind tunnel tests in a scaled-down model of an existing industrial facility. The experiments were performed as part of the EMU-project (Evaluation of Modeling Uncertainty) which was a European collaboration performed under the CEC Third Framework Programme in 1994-1997. The experimental data were later adapted for use in model validation by the SMEDIS (Scientific Model Evaluation for Dense gas dISpersion models) performed under the CEC Fourth Framework Programme in 1997-1999.

The scenario was simulated both with a complex CFD (computational fluid dynamics) model [1, 2] and with simplified phenomenological models, and the computed results were compared against the EMU/SMEDIS data set.

FLUENT is a fully featured CFD package that can be applied to simulate a wide range of fluid dynamics phenomena, among them the release and dispersion of a contaminant in air.

Hazard Prediction and Assessment Capability (HPAC) is a military decision support system to assess a wide range of CBRN incidents. HPAC is developed by the Defense Threat Reduction Agency (DTRA), and is in operational use by the armed forces of several nations, most notably the US army. The dispersion kernel of HPAC is based on the SCIPUFF Gaussian model which has been extended to take into account negatively or positively buoyant contaminants [3, 4].

2 Scenario description

The scenario describes the release of gaseous chlorine from a storage vessel in an industrial compound. Such a scenario could be realized and pose a threat both as an accident involving a valve break or partial tank failure, or by a small-scale attack on the facility by military, para-military or criminal elements.

The release takes place inside the industrial compound. The site is located on a plateau in a shallow valley bordering the sea. To the north of the site there are steep cliffs leading down to the sea. The floor of the valley slopes gently upwards from height of approx. 16m above sea level at the release point to approx. 21m above sea level to the south. To the east and the west, the terrain rises to a height of approx. 26m above sea level.

Detailed information is available describing both the location, size and shape of the buildings within the facility, and the topography in the area surrounding the installation in the form of elevation data in a 10m-by-10m grid. In Figure 2.1 we show the lay-out of the installation, and in Figure 2.2 we show a computer representation of the installation and the surrounding terrain. The wind direction is from North, i.e. from the direction of the sea, with a wind speed of 5m/s. A 10% chlorine-in-air mixture is released in a jet that is directed 45° away from the main wind direction. The release flow rate was 230 kg/s, corresponding to a jet velocity of approx 70 m/s.

A scaled-down model of the installation and the surrounding countryside was constructed and wind-tunnel experiments were performed during the EMU (Evaluation of Model Uncertainty) project [5]. The experimental data was later post-processed, scaled back to real scale, and used as a test case in the SMEDIS project (Scientific Model Evaluation for Dense gas dISperson models). We give a detailed specification of the release scenario in Table 2.1.

3 FLUENT simulations

FLUENT is a fully featured CFD (Computational Fluid Dynamics) code that can be applied to the computation of a large range of fluid dynamics phenomena, including the release and dispersion of

Table 2.1: Release scenario specification. The symbols (+) indicate which data were used to specify the simulations for the two models.

		CFD	HPAC
Substance	Cl ₂	+	+
Release type (puff/jet/cyclone)	jet	+	
Obstacle configuration	file: bld.txt	+	
Nozzle diameter (m)	1.74	+	(+)
Pool mass fraction	0		
Release point (x,y,z)	(0,0,0)	+	+
Release direction, α	315	+	
Release elevation, β	0	+	
Phase (liquid to gas mass ratio)	0		
Initial volume fraction	0.1	+	
Initial mass fraction	0.214		
Exit temperature (°C)	20		
Release rate (kg/s)	230	+	49kg/s pure Cl ₂
Release start time (h,m,s)	(0,0,0)		
Release duration (s)	900s	+	+
Site avg wind direction (deg from N)	0	+	+
Ideal wind direction (deg from N)	0		
X-axis orientation (deg from N)	0		
Site average wind speed (m/s)	5	+	+
Reference height for wind (m)	10		
Wind speed standard deviation (m/s)	0.55		
Friction velocity (m/s)	0.47		
Surface roughness at site(m)	0.1	+	internal map data
Surface roughness at water (m)	0.075		internal map data
Stability class	D		+
Ambient temperature (°C)	20		+
Ground slope	file: amlwch.exe	+	internal map data
Molecular weight (g/mol)	70.6		

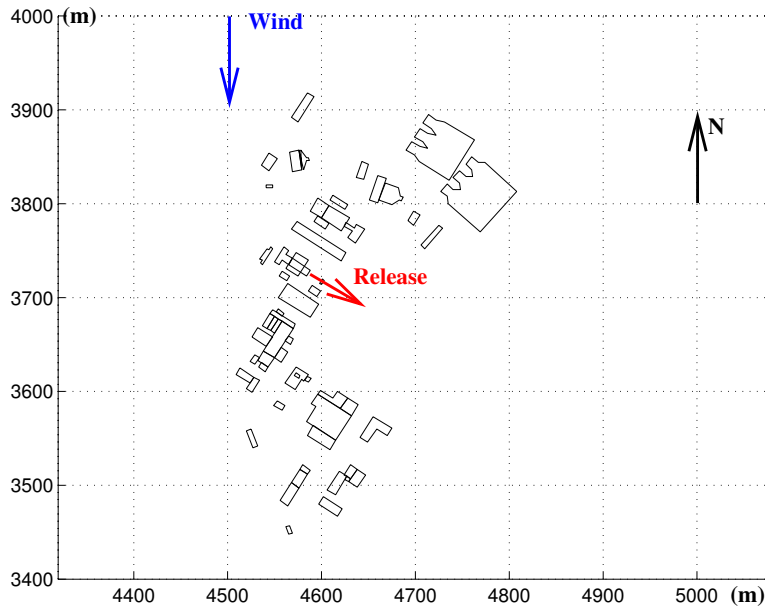


Figure 2.1: Schematic lay-out of the buildings in the industrial facility.

contaminants in air. We have performed a series of simulations of the reference scenario [1, 2].

To simulate contaminant transport, FLUENT solves the Navier-Stokes equations, that govern fluid flows, augmented by a scalar equation for the contaminant concentration and model equations to take into account the effects of turbulence. Since chlorine is significantly heavier than air, the mixture density, and hence the flow field, will be affected by the contaminant.

3.1 Geometry and grid

The simulation covers an area spanning $500\text{m} \times 600\text{m}$. In this area, topographical data are given with $10\text{m} \times 10\text{m}$ resolution. The height of the computational box was chosen at $z = 300\text{m}$ so that the upper boundary is outside the boundary layer and does not influence the wind field at ground level where the dispersion takes place. The altitude of the terrain varies by approx 30m ; the effective height of the computational domain is therefore in the range 270m – 300m .

The computational domain was discretized with an unstructured mesh using tetrahedral cells. In the area inside the facility close to the release we attempted to use fairly regular grid spacing, ranging from approx. 1m for the finest resolution to approx. 7m for the coarsest resolution. We performed five simulations in total with the number of grid cells for each simulation in the range 3 million to 15 million. The buildings at the site were completely represented in all simulations. In four of the performed simulations we used the topographical data supplied for the site, whereas for one simulation we used a flat terrain. The grid parameters for the different runs are summarized in Table 3.1.

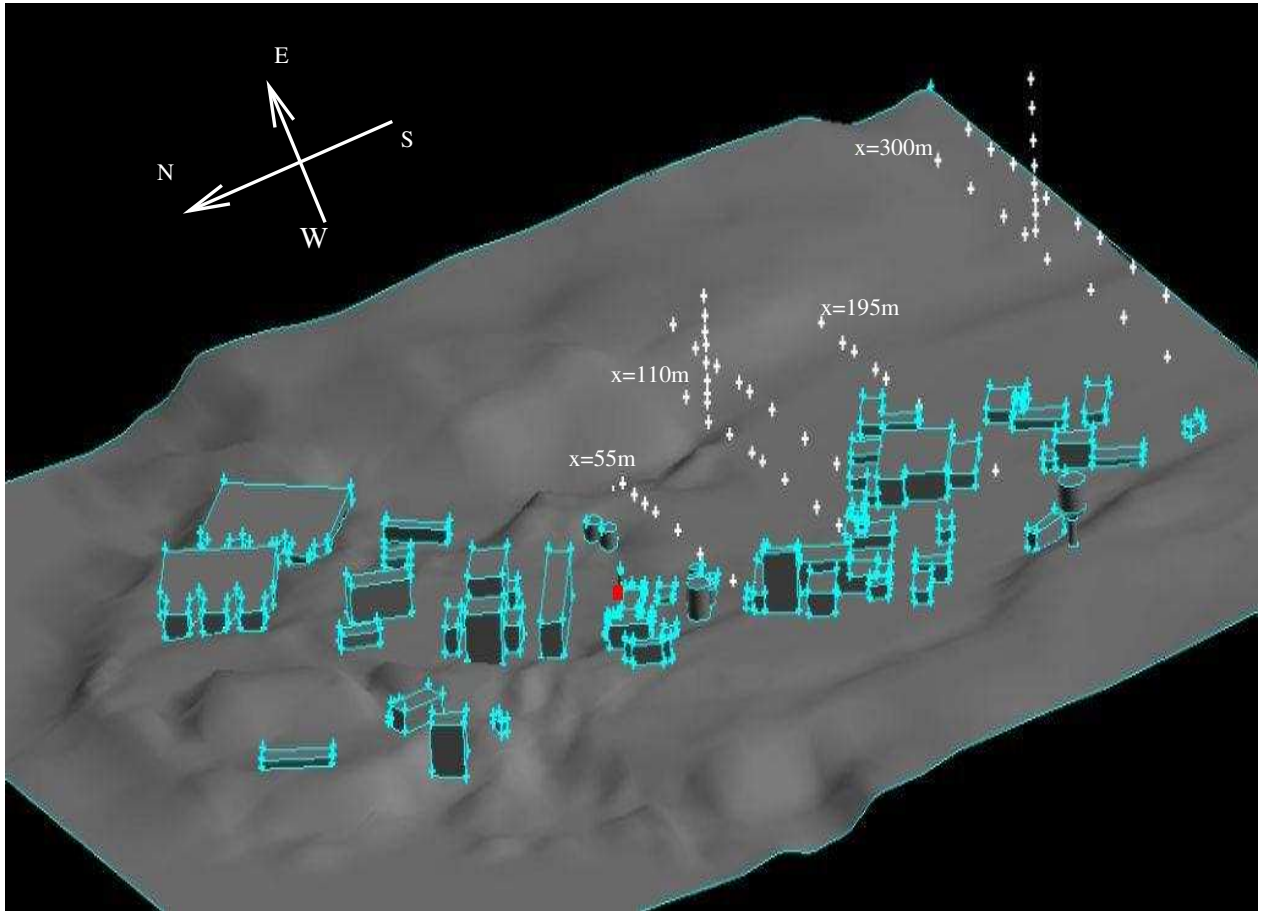


Figure 2.2: Computer representation of the industrial facility and the surrounding terrain. The red point marks the release point, and the white markers show measurement locations. The indicated distances are downwind relative to the release point.

Table 3.1: Geometry and grid specification for the FLUENT simulation

Run ID	Geometry	Topography	Grid spacing at facility	No. of cells
1	Full	Real	7m	3.0 million
2	Full	Real	2m	6.8 million
3	Full	Real	1m	14.8 million
4	Full	Flat	2m	9.3 million
5	Full	Real	7m	3.0 million

Case 1 and Case 5 use the same mesh, but the release point was raised vertically by approx 1m in Case 5.

3.2 Turbulence model and boundary conditions

To take into account turbulence effects, we used the $k - \omega$ model with standard model parameters. The roughness length was set to $z_0 = 0.1\text{m}$ both for the ground and for the small area of the lower surface that was over the sea. The incident wind is from the North, i.e. parallel to the length of the computational domain, and was specified as a constant velocity across the entire inflow face. We assume that the turbulence generated by the interaction of the wind with the cliffs and the bluff buildings will dominate the local turbulence field, and hence the dispersion. For the boundaries parallel to the flow we use symmetry (i.e. free slip) boundary conditions.

3.3 Simulations

The simulations were performed using a second order accurate advection scheme for the momentum and concentration equations. For the turbulence fields, k and ω , we used a first order scheme to ensure the stability of the simulation.

For each case, we performed an initial simulation to establish the wind field. For the coarsest meshes we converged the solution to steady state. For the finest mesh, the flow field did not converge to a steady state and we computed the initial wind field by solving the time-dependent equations until we reached a representative state.

We computed the release as a 900s transient simulation, and recorded time histories of contaminant concentration at 66 monitor points. The time histories were then averaged over the entire duration of the release and compared with the experimental data set.

3.4 Simulation results

In this chapter we will present the results of the simulation. We will discuss the overall performance of the simulations compared to the reference data, using established statistical techniques. We will also look into concentration profiles in the plume and compare simulated and experimental data in the sensor locations.

In the experiments, time histories of chlorine concentration were recorded in 66 sensor locations laid out in horizontal and vertical rows, shown in Fig. 2.2, as follows:

- Four horizontal rows at ground level, located 55m, 110m, 195m, and 300m downwind of the release.
- Two horizontal rows approx 19m above ground level, located at 110m and 300m downwind of the release.
- Two vertical towers located at 110m and 300m.

The EMU/SMEDIS data sets comprises mean values from these sensors, averaged over the 900s duration of the release. We recorded the same data for each simulation, and normalized the data according to Eq. (3.1) below.

In order to compare the scaled-down wind tunnel tests with simulations that are performed at full scale, the experimental data is normalized with a reference concentration defined by

$$C^* = \frac{C_s Q_s}{U_H H^2}, \quad (3.1)$$

where C_s is the contaminant concentration in the release, Q_s is the release rate, H is the average building height, and U_H is the wind speed at the average building height [5]. For the full scale, we also calculated a reference C^* , and the simulated results were also normalized by this C^* and expressed in non-dimensional form to be comparable to the experimental data.

3.4.1 Statistical analysis

In this section we will consider the overall performance of the simulations by using statistical performance measures to compare the simulated and experimental data sets. A large number of statistical performance measures have been proposed and used to evaluate dispersion models. The SMEDIS project reviewed several methods in [6]. We will perform the comparison using the metrics *Factor of two* (FA2), *Mean Relative Bias* (MRB), and *Mean Relative Square Error* (MRSE) in line with the recommendations of the SMEDIS project.

In the following discussion we assume we have a set of predictions and observations, denoted by C'_p and C'_o , respectively. Measurement positions that lie close to the edge of the plume can make a disproportionately large impact on the computed values of the statistical performance measures. To overcome this, we can set a threshold value and process the data such that all values that are smaller than the threshold is set to the threshold value. Mathematically, we can write

$$C = \max(C', C_{\text{thresh}}),$$

where C is the processed value that will be used in the comparison. The threshold value is sometimes chosen to be related to the sensitivity of the instruments used to obtain the measurements. In the present work, we employed the same threshold as in the SMEDIS project, viz. $C_{\text{thresh}} = 10^{-3}$.

The results of dispersion models have traditionally been considered adequate if they give results within a factor of two of the reference data, i.e. if we have

$$C_o/2 \leq C_p \leq 2C_o.$$

The FA2 performance measure is defined as the fraction of monitor locations where this holds

$$\text{FA2} = \frac{N|_{C_o/2 \leq C_p \leq 2C_o}}{N_{\text{tot}}}.$$

Table 3.2: Factor of two (FA2) values for the five simulated cases

Case:	Raw data	With thresholding
1	0.15	0.20
2	0.29	0.33
3	0.46	0.49
4	0.42	0.47
5	0.18	0.22

The computed FA2 for the five simulations are given in Table 3.2. In general we see improved results with increasing resolution.

The FA2 metric only tells us the fraction of the measurements that lie within the factor-of-two band. To obtain more information, we must also look at other metrics. The Mean Relative Bias (MRB) is a measure of over- or under-prediction that is defined by

$$\text{MRB} = 2 \overline{\left(\frac{C_p - C_o}{C_p + C_o} \right)},$$

where the over-bar denotes an average over the entire data set. Note that negative MRB values imply under-prediction, and that positive MRB values consequently imply over-prediction. A closely related metric is the Mean Relative Square Error (MRSE), which is related to the variance of the difference between the compared data sets and is thus a measure of the scatter in the comparison of the predicted and observed values. The MRSE is defined by

$$\text{MRSE} = 4 \overline{\left(\frac{C_p - C_o}{C_p + C_o} \right)^2},$$

When considered together, the MRB/MRSE pair gives information both on the level of over- and under-prediction and to what extent the predictions are consistent with the observations. We can show this by noting that we always have

$$\text{MRSE} \geq \text{MRB}^2,$$

with equality in the case that the model over- or under-predicts with the same factor in all monitor locations. If we plot MRB vs. MRSE there will be an 'ideal' trend curve given by the parabola $y = x^2$. The extent that a model result is consistent with the reference data can be assessed by the distance to the trend curve. We show MRB and MRSE of the five simulations, both with and without thresholding, in Figure 3.1. In general we see improved results with better resolution, as expected. The effect of thresholding is apparent; the majority of points are not affected, but for points that are close to the plume edge (i.e. with concentrations close to zero) small differences of little real significance give a large contribution to the computed metrics. Note that both thresholding and grid refinements move points more or less parallel to the trend curve, giving confidence that the simulations are, in a sense, consistent with the experimental data.

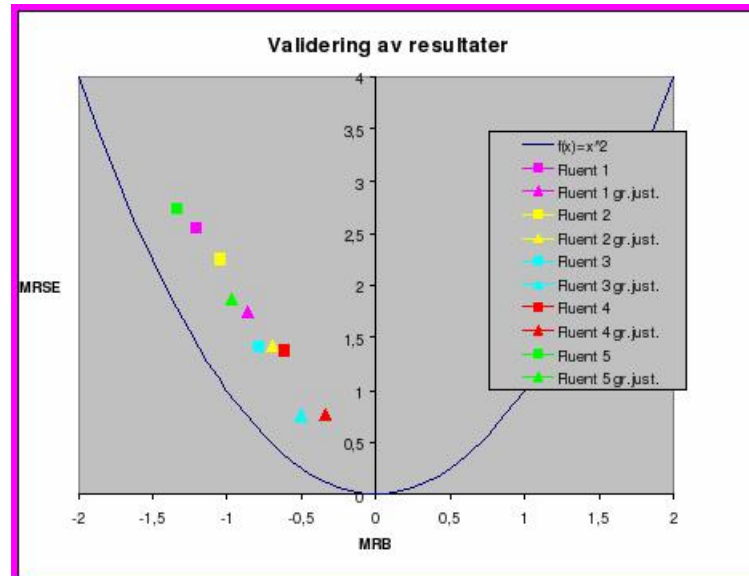


Figure 3.1: Statistical performance measures, MRB vs. MRSE, for the simulations. Squares show the metrics computed based on the raw data, whereas the triangles show the metrics computed with data that have been processed by thresholding.

The same data set was used in the SMEDIS project [7] to compare results from a large number of dense gas dispersion models, both CFD models and phenomenological models. In Figure 3.2 we compare the results from the present simulation with results from comparable general-purpose CFD models submitted to the SMEDIS project¹. There is a larger scatter in the SMEDIS results, probably caused by the larger diversity both with respect to models and operators. The present simulations performs comparably or better than the older SMEDIS results. Parts of the observed improvement can surely be attributed to the greater availability of computing resources and hence the ability to simulate with greater resolution.

3.4.2 Plume profiles

In Fig. 3.3 and Fig. 3.4 we show a snapshot of the plume at ground level at the end of the 900s simulation for Case1 and Case3, that is the coarsest and finest simulations, respectively. Note that in Case1 we obtain a narrow and fairly straight plume, whereas in Case3 the plume is wider and wavier. This can be interpreted that the simulations in Case1 resulted in a steady- (or almost steady-) state giving the narrow plume, and that the wider plume and wavy structures in Case3 represents a case of unsteady dispersion caused by large-scale shedding downstream of the facility. To investigate this hypothesis we show, in Fig. 3.5, the recorded time history of concentration for the two cases in a monitor location in the row of sensors located 300m downwind of the release. Case1 is indeed characterized by small fluctuations about a mean value, showing that the flow and dispersion is

¹B. Carissimo, private communication

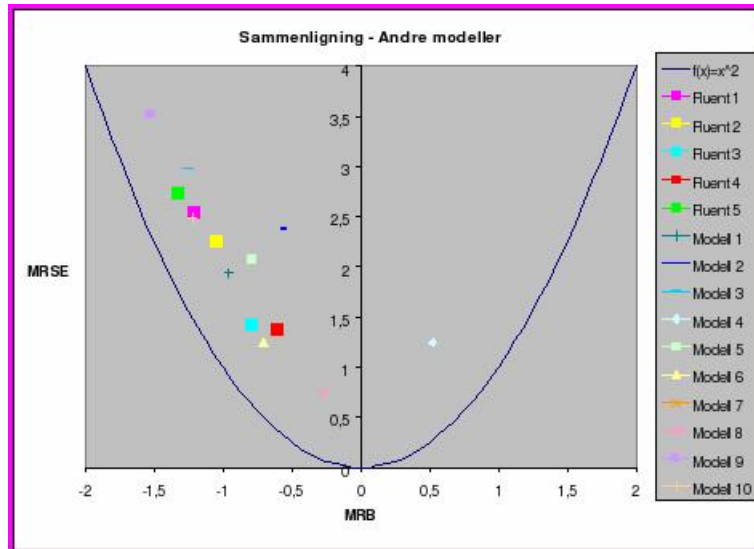


Figure 3.2: Statistical performance measures, MRB vs. MRSE, for the present simulations compared with results from the SMEDIS project.

close to stationary. For Case3 we observe unsteady motion with a period of about 30s. Note that unsteady mixing is a very efficient dispersion mechanism that explains the wider plume in Case3. These effects can not be captured in steady-state simulations.

The reason that the coarser simulations give a wind field and dispersion pattern that is close to stationary is that unsteady effects are effectively damped by the larger numerical dissipation inherent in the coarser discretization. Recall that in the finest simulation, Case3, we did not manage to converge the wind field to a steady state prior to the dispersion calculation.

3.4.3 Horizontal downwind profiles

In Fig. 3.6 we show the computed maximum concentration along the plume for the five simulations compared to the experimental reference. All five simulations over-predict the maximum concentration. The along-plume concentration level and decay are roughly comparable to the reference data for all the cases.

3.4.4 Horizontal cross-plume profiles

In Figs. 3.7–3.10 we show the horizontal cross-plume concentration profiles for both the experiment and the simulation. In general, we see that the plume is narrower for all simulations compared to the reference data. This applies especially to the sensor rows at ground level, but can also be seen in the two sensor rows located at 19m height. As a consequence, the maximal concentration is higher in the simulations than in the reference.

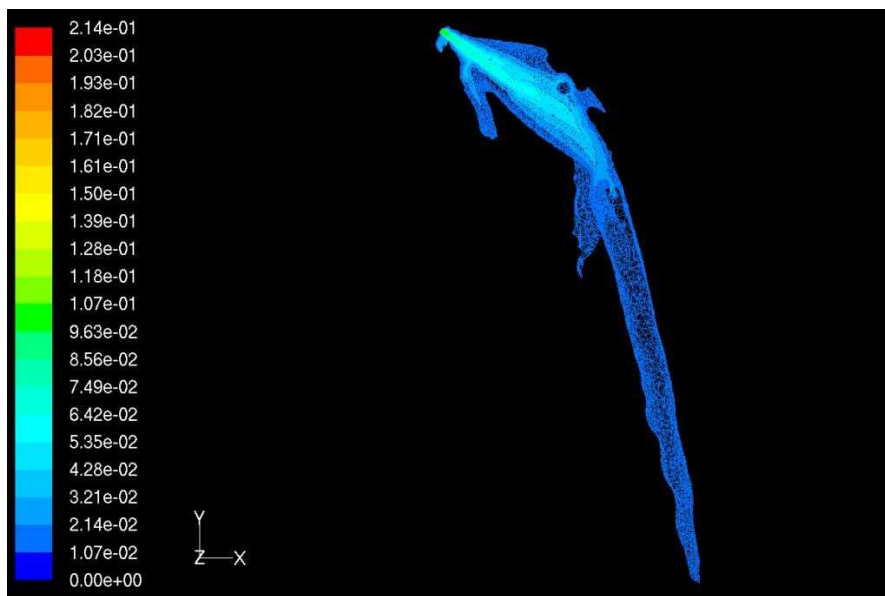


Figure 3.3: Plume profile at the end of 900s simulation for Case 1 with approx three million cells. North is in the positive y -direction, and East is in the positive x -direction.

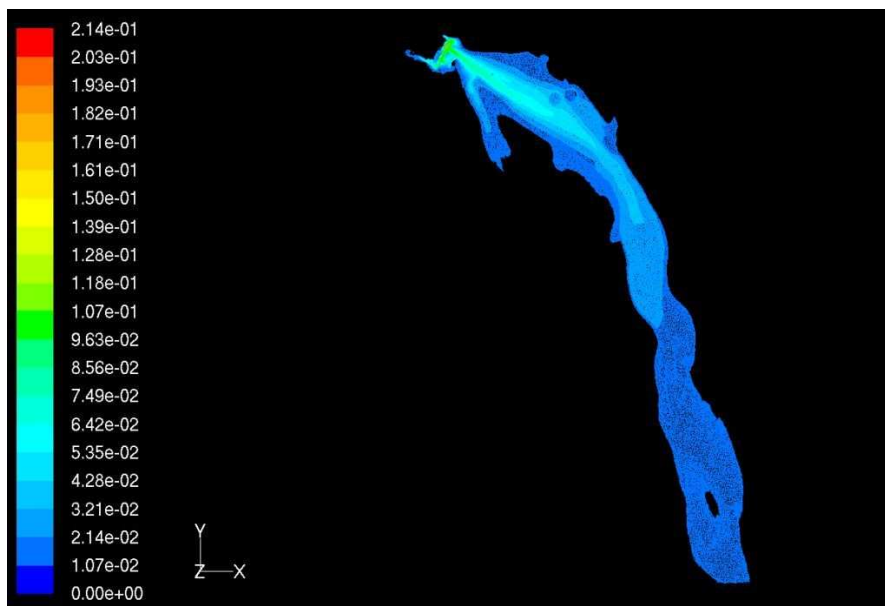


Figure 3.4: Plume profile at the end of 900s simulation for Case 3 with approx 15 million cells. North is in the positive y -direction, and East is in the positive x -direction.

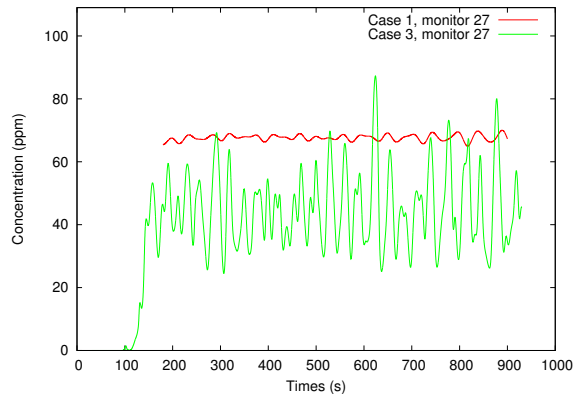


Figure 3.5: Time histories of concentration for a monitor at the plume centreline of the sensor row located at ground level 300m downwind of the release. Case1 and Case3, respectively.

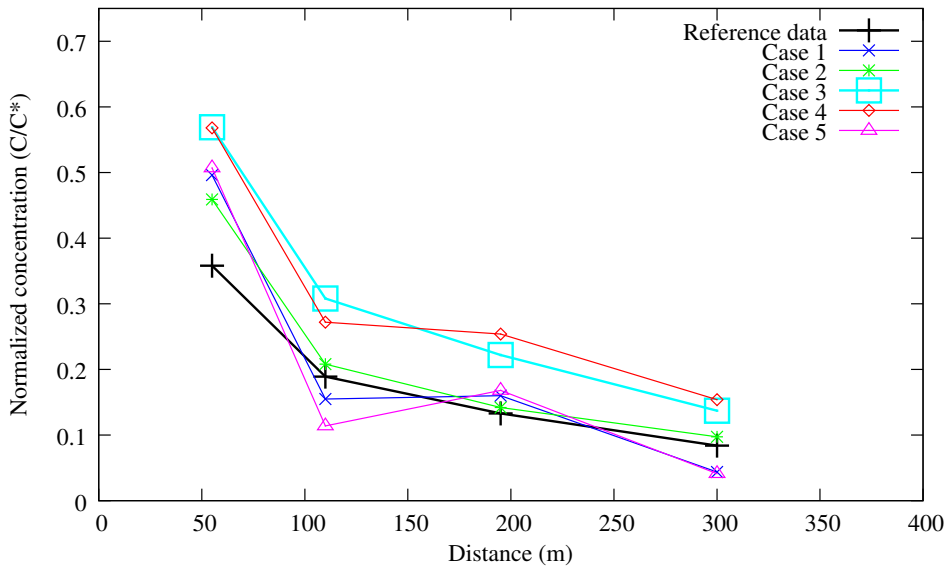


Figure 3.6: Maximum concentration at ground level downwind from the release. The downwind distance is measured along the wind direction and not along the plume.

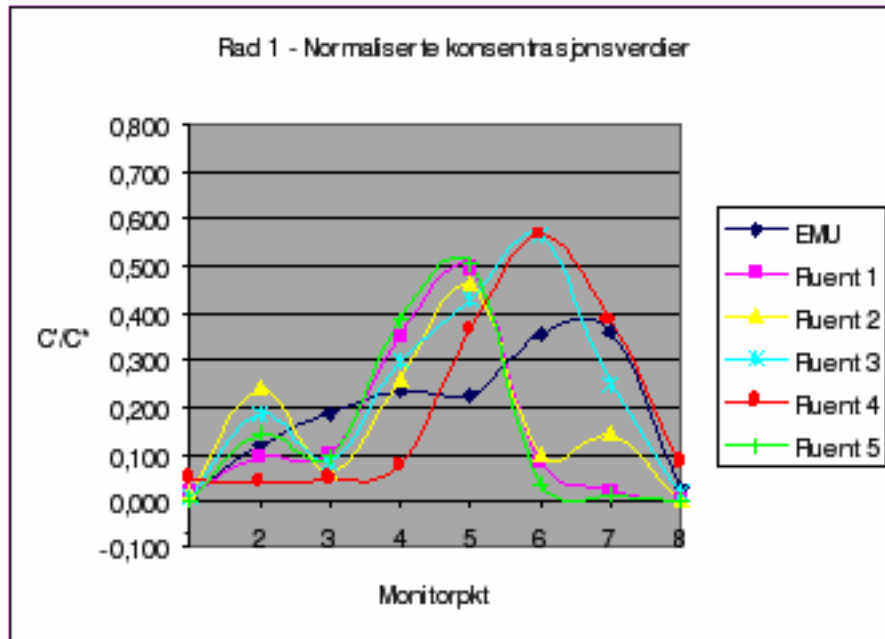


Figure 3.7: Averaged cross-plume concentration profiles at a sensor row located at ground level – $z = 0 - 55m$ downwind of the release. The monitor points are numbered from west to east relative to the sensor row.

Consistent with the statistical analysis above, Case3 appears to show the best overall performance. This is the only case in which the location of the peak concentration coincides with the reference data for all the horizontal sensor rows. It is also the case with plume width closest to the reference for all rows, although the plume width is still underestimated. Case4, which is a coarser simulation performed at a flat surface, also corresponds well with the reference, both with respect to location of the peak and plume width, in the near field. There are however larger discrepancies further downstream in this case. This indicates that the effect of buildings is relatively more important in the near field whereas topography is more important in the far field, which appears to be a plausible observation.

3.4.5 Vertical cross-plume profiles

We show the average vertical concentration profiles from two towers located 110m and 300m downstream of the release in Fig. 3.11 and Fig. 3.12. These measurements are of course very sensitive to the plume trajectory, and we note that for the coarse simulations (Case1, Case2, and Case5) the plume misses these locations completely. The remaining cases, the finest simulation (Case3) and the flat simulation (Case4), show qualitative agreement with the reference data.

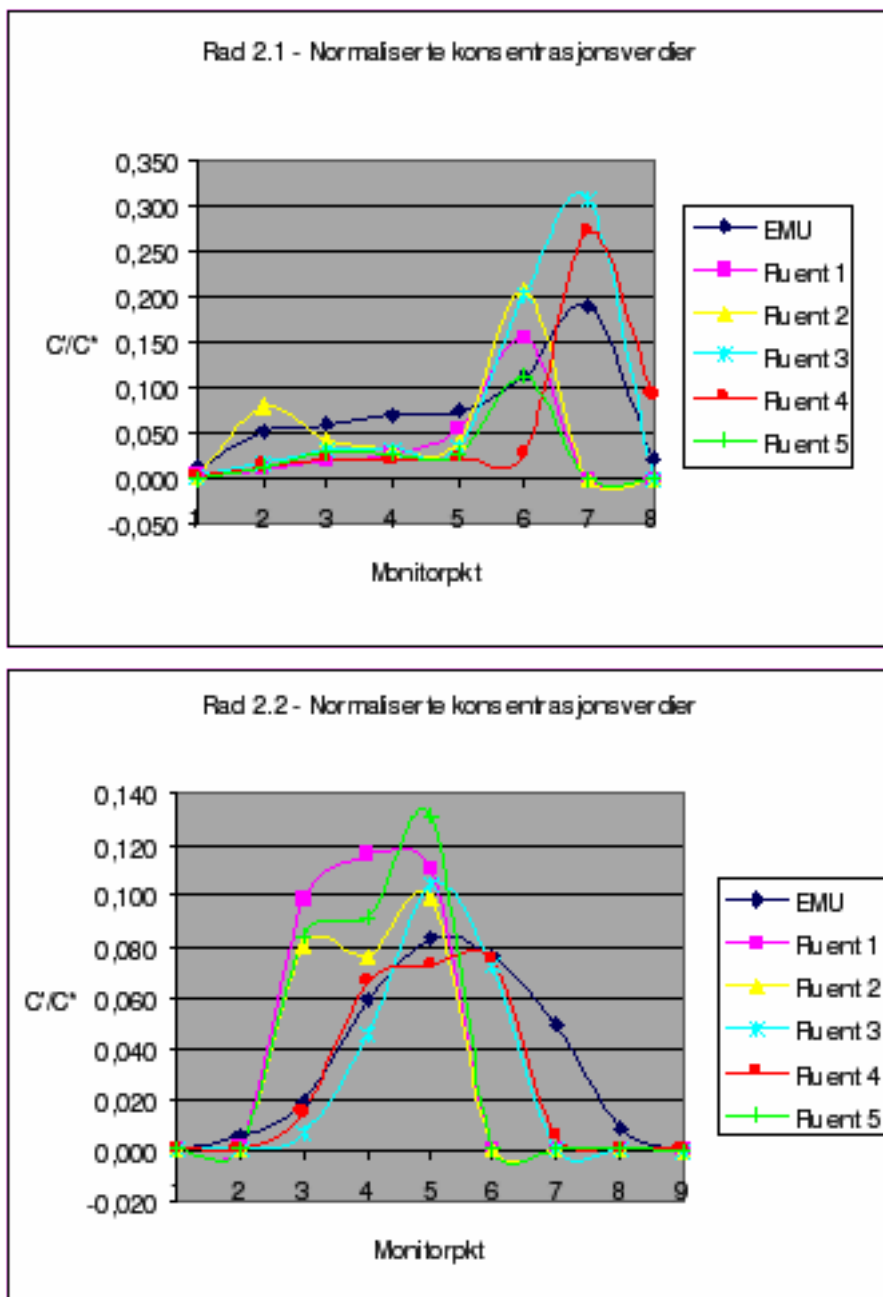


Figure 3.8: Averaged cross-plume concentration profiles at two sensor rows located at different heights – $z = 0.25\text{m}$ (top) and $z = 18.8\text{m}$ (bottom) – 110m downwind of the release. The monitor points are numbered from west to east relative to the sensor row.

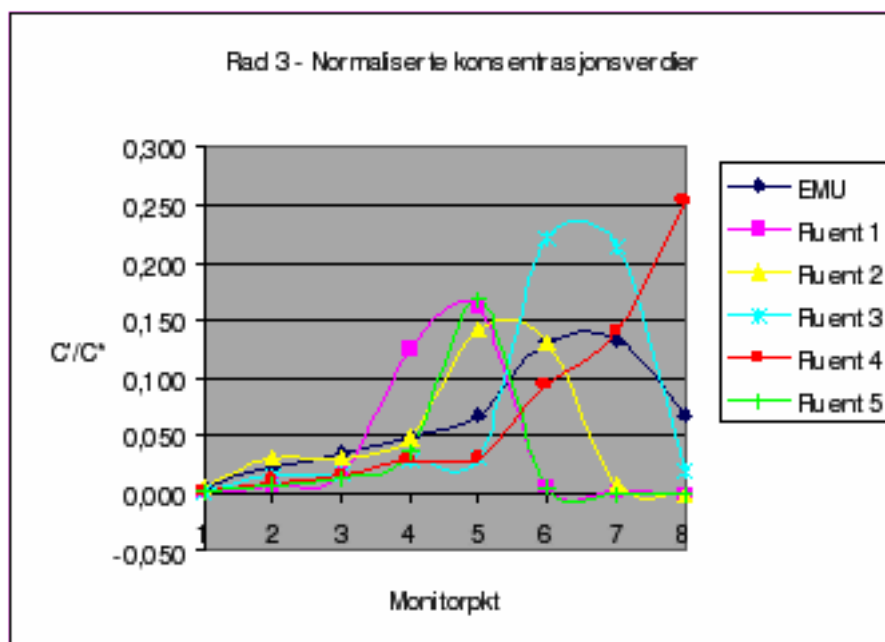


Figure 3.9: Averaged cross-plume concentration profiles at a sensor row located at ground level, $z = 0$, 195m downwind of the release. The monitor points are numbered from west to east relative to the sensor row.

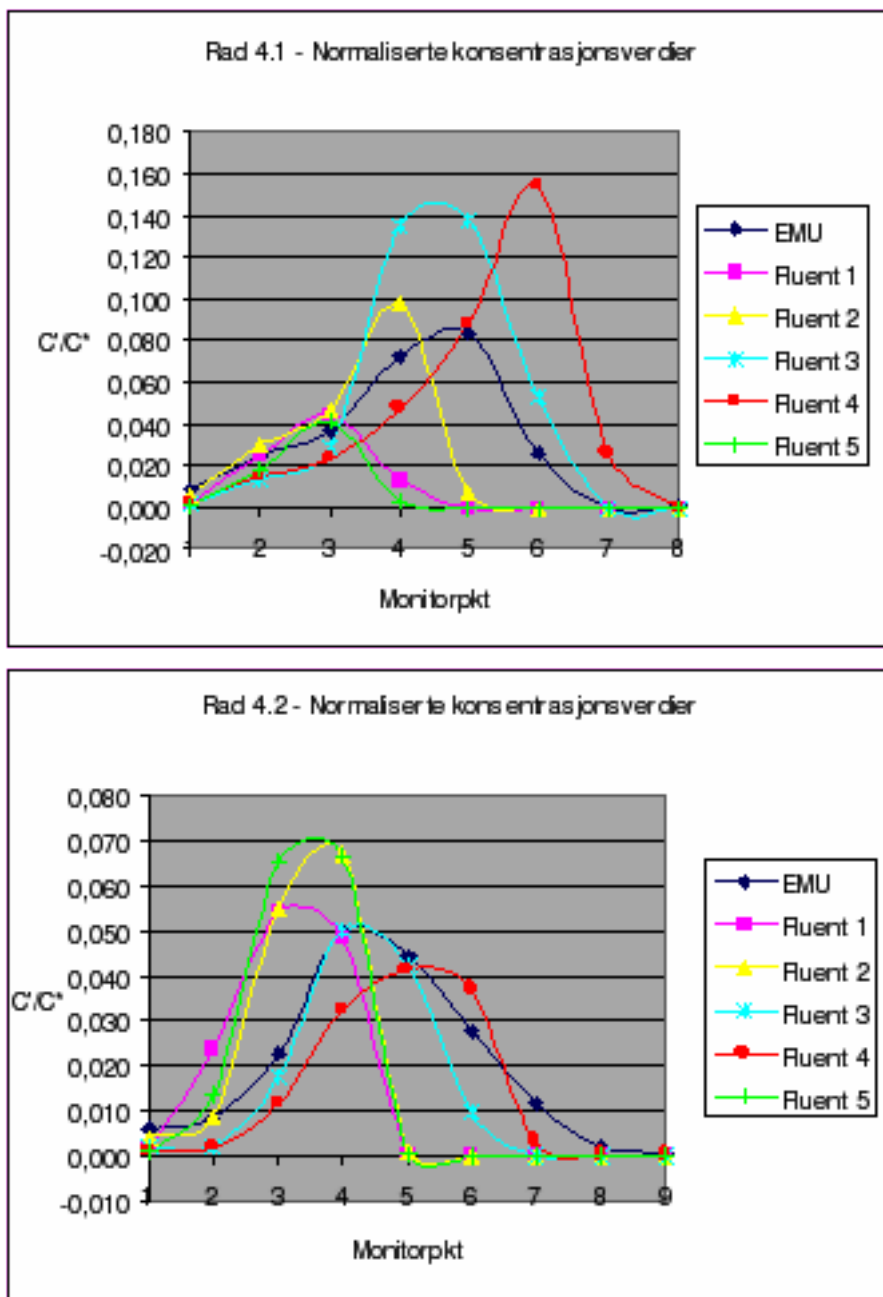


Figure 3.10: Averaged cross-plume concentration profiles at two sensor rows located at different heights – $z = 0.25\text{m}$ (top) and $z = 18.8\text{m}$ (bottom) – 110m downwind of the release. The monitor points are numbered from west to east relative to the sensor row.

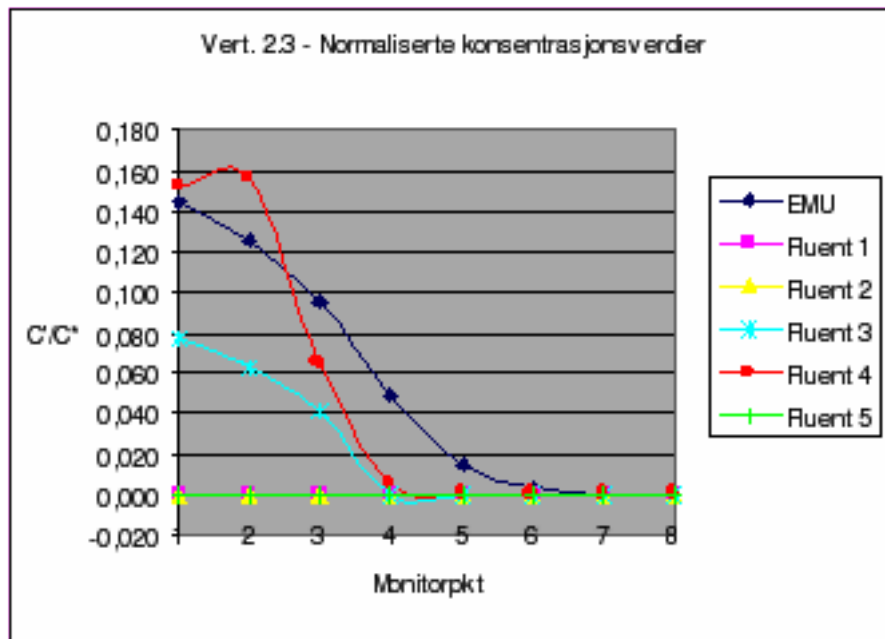


Figure 3.11: Averaged vertical concentration profiles at sensors located 110m downwind of the release. Monitors are numbered with increasing height and are located from $z = 6m$ to $z = 39m$ above ground level.

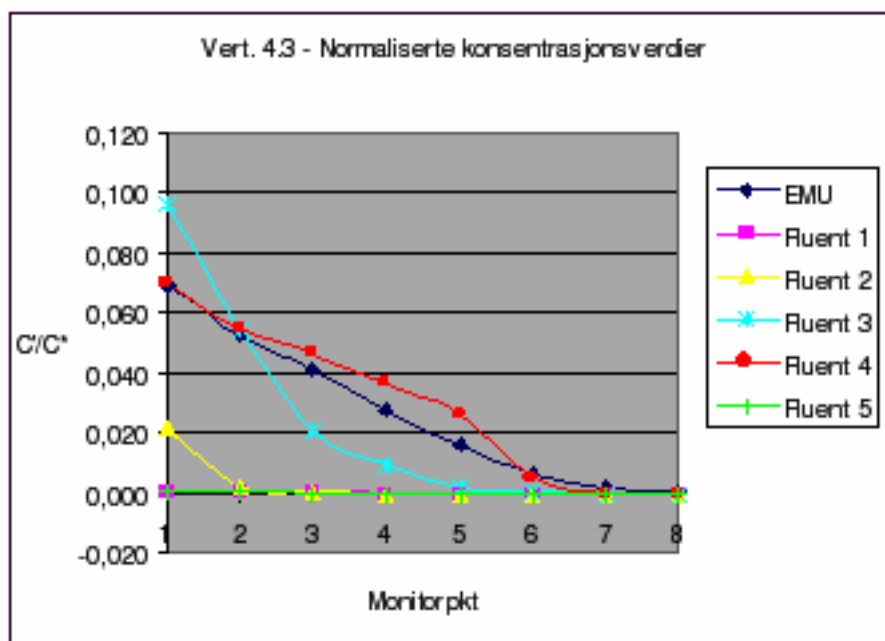


Figure 3.12: Averaged vertical concentration profiles at sensors located 300m downwind of the release. Monitors are numbered with increasing height and are located from $z = 4m$ to $z = 51m$ above ground level.

4 HPAC model results

HPAC (Hazard Prediction and Assessment Capability) is a military decision support system to assess a wide range of CBRN incidents. HPAC is developed by Defense Threat Reduction Agency (DTRA). The dispersion kernel in HPAC is based on a Gaussian puff model (SCIPUFF) in which the contaminant plume is represented as a superposition of discrete puffs (sub-clouds) that are transported by the ambient wind field and take into account the motion of negatively or positively buoyant contaminants [3, 4].

4.1 Simulation set-up

The release is represented in HPAC's analytic module as a continuous source of pure chlorine with a rate of approx. 49kg/s. Note that the experimental data set is based on a 270kg/s release of a 10% chlorine-in-air mixture. HPAC can however only represent release of pure substances.

Although HPAC can handle vertical jet release, it does not have the capability to represent a horizontal directed jet. As a consequence, deflection of the plume caused by the initial momentum of the jet will not be predicted by HPAC. Furthermore there is no representation of building geometry in the model, and plume-building interactions are therefore not accounted for.

The height of the release point was set to $h = 1\text{m}$. In [4], the initial σ -value for a vertical jet release were chosen as $\sigma = r$, where r is the radius of the jet. In line with this, we choose

$$\sigma = 0.87\text{m},$$

for the present simulation. Thus, are the radius of the initial puffs comparable to the radius of the expanded jet.

The atmospheric stability was set to neutral (Pasquill class D), the wind velocity to 5m/s, and the temperature to 20°C.

We performed simulation both for a flat terrain and for the real topography as supplied by HPAC's internal map data base. The resolution of these data appears to be approx 1000m × 1500m, so the HPAC simulations can not expect to capture the same level of detail as the FLUENT simulations, in which we used topographic data with 10m × 10m resolution.

4.2 Simulation results

Since HPAC can not take into account deflection of the plume by the momentum of the release jet, the plume is directed along and symmetric about the wind direction as we show in Fig. 4.1. We can therefore not perform a direct comparison of the HPAC results with the experimental data set.

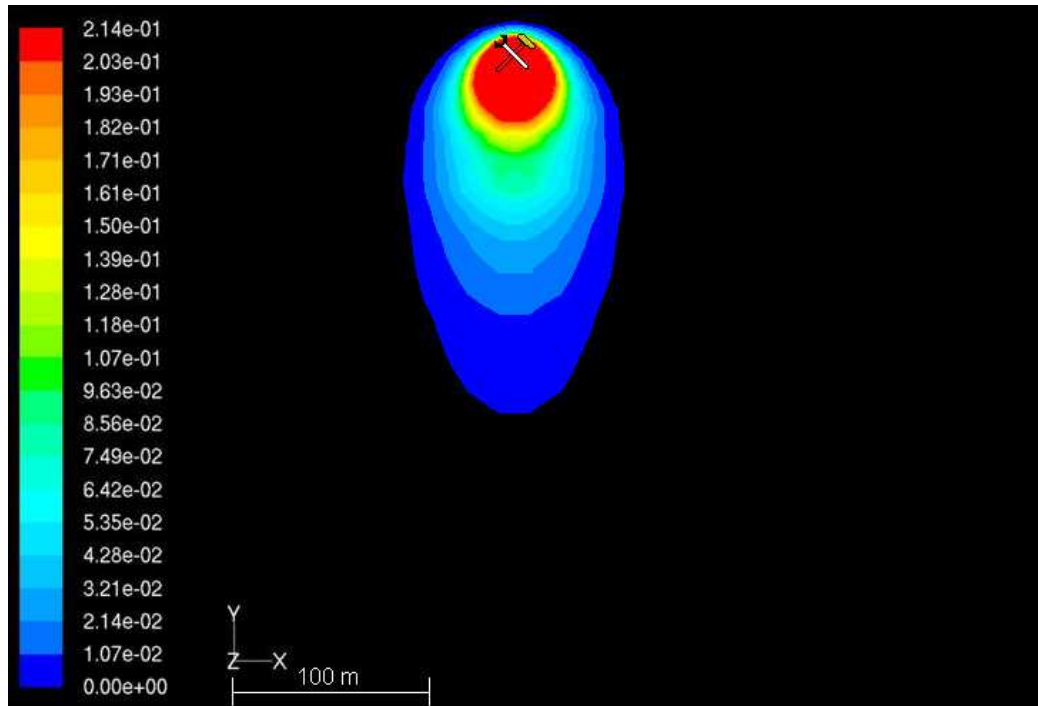


Figure 4.1: HPAC Prediction of the chlorine plume at the end of the 900s release.

We can however do a qualitative comparison, for example of maximum concentrations and plume width.

Chlorine concentration was recorded at several monitor points along four horizontal rows at ground level, located 55m, 110m, 195m, 300m, 450m, and 675m downwind of the release. The recorded time series were then averaged over the release duration $t = 900\text{s}$ and normalized, according to Eq. (3.1), for comparison with the reference data.

4.2.1 Downwind profiles

In Fig. 4.2 we show the computed maximum concentration along the plume both for the two HPAC simulations, with and without topography, and for the experimental data. Note that the HPAC simulations appear to show a more rapid dilution of the concentration than observed in the experiments. In the near field, the distance from the release to the point where the concentration reaches a certain level may vary by a factor of two between the model results and the reference. In the intermediate to far field this distance may be smaller. Note however that the model appears to under-predict in the far field while it is conservative close to the source.

The most important free parameter in the SCIPUFF model used in HPAC is the initial puff parameter σ . As we noted above, σ was chosen to be comparable to the radius of the release jet. In Fig. 4.3 we show the sensitivity of the maximum downwind concentration profile to the choice of this parameter. Choosing either the radius or the diameter of the jet for the puff parameter result in small differences

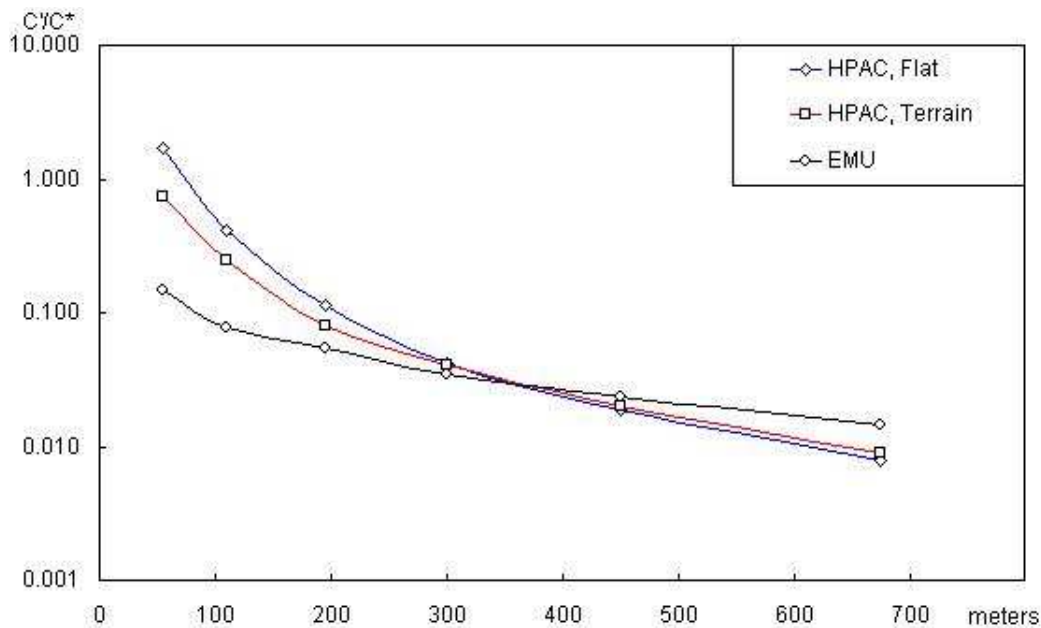


Figure 4.2: Maximum concentration along the plume at ground level for HPAC simulations compared to the experimental reference data.

in the computed results. Smaller values do however result in much higher near field concentrations and more rapid dilution. The near field concentration is much too high in all these cases. We also tried to vary the lateral puff parameter, σ in order to match the contaminant concentration in the release. In Fig. 4.4 we see that we need to choose $\sigma > 25\text{m}$ to achieve this. Such a large σ bears no relation to any physical scale relevant to the release. The decay of the maximum concentration profile is still much too rapid, leading to under-prediction at all distances. The resulting plume will also be much too wide because of the large value of σ .

4.2.2 Cross-wind profiles

In Figs. 4.5–4.10 we show the cross-plume concentration profile at ground level for each of the horizontal rows located downstream between 55m and 675m. We note that the chlorine concentration is larger than the reference values in the near field and smaller than the reference in the far field, in line with the centreline concentration plots shown above. The plume widths predicted with HPAC appear to be significantly larger than the reference data in the near field, whereas plume widths are comparable to the reference data further downstream. As we also observed in the previous section, concentrations levels decay more rapidly in the HPAC simulations.

Most of the observed differences can probably be explained by the lack of a model to account for the momentum-driven jet release. A directed jet release will naturally lead to a narrower plume close to the source, and turbulent entrainment will tend to dilute the near field plume and thus reduce over-prediction.

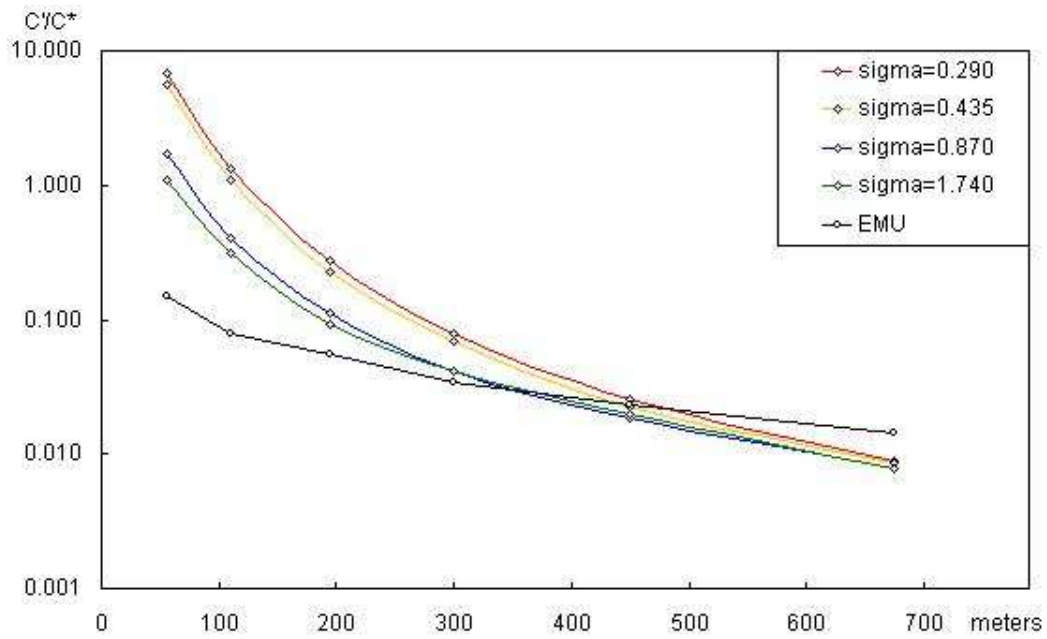


Figure 4.3: Maximum concentration along the plume at ground level for HPAC simulations compared to the experimental reference data. Dependence of the σ parameter.

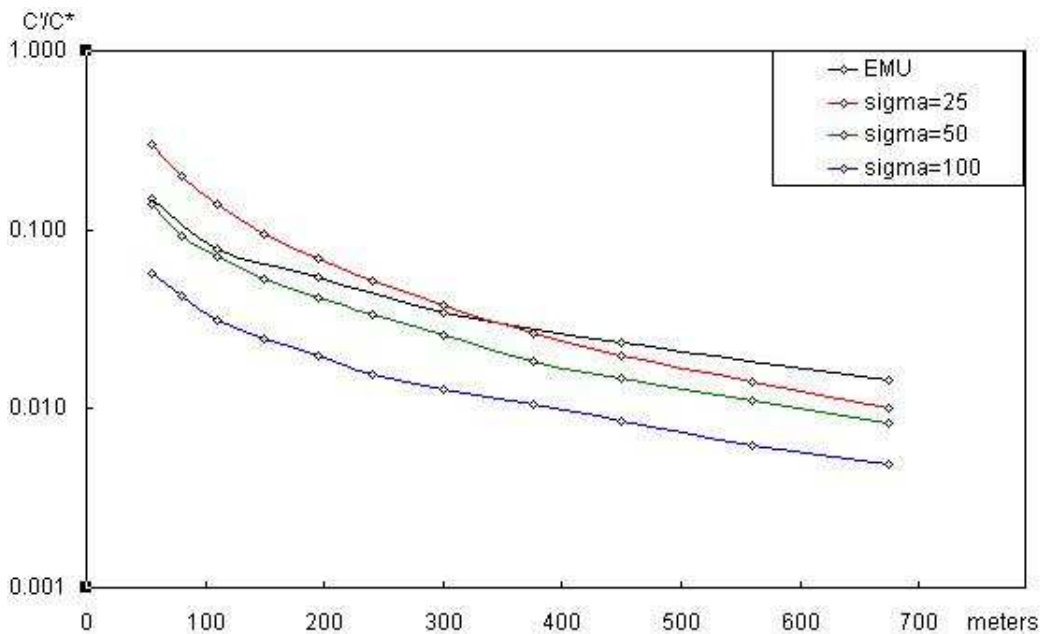


Figure 4.4: Maximum concentration along the plume at ground level for HPAC simulations compared to the experimental reference data. Dependence of the σ parameter.

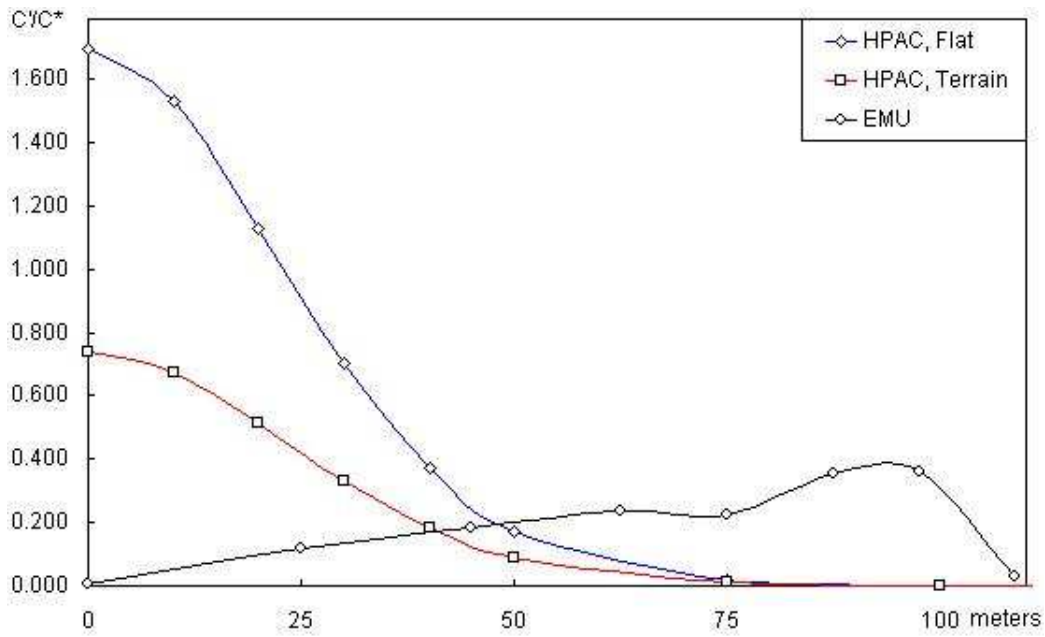


Figure 4.5: Cross-plume concentration profile at ground level, 55m downstream of the release. HPAC simulations compared to the experimental reference data.

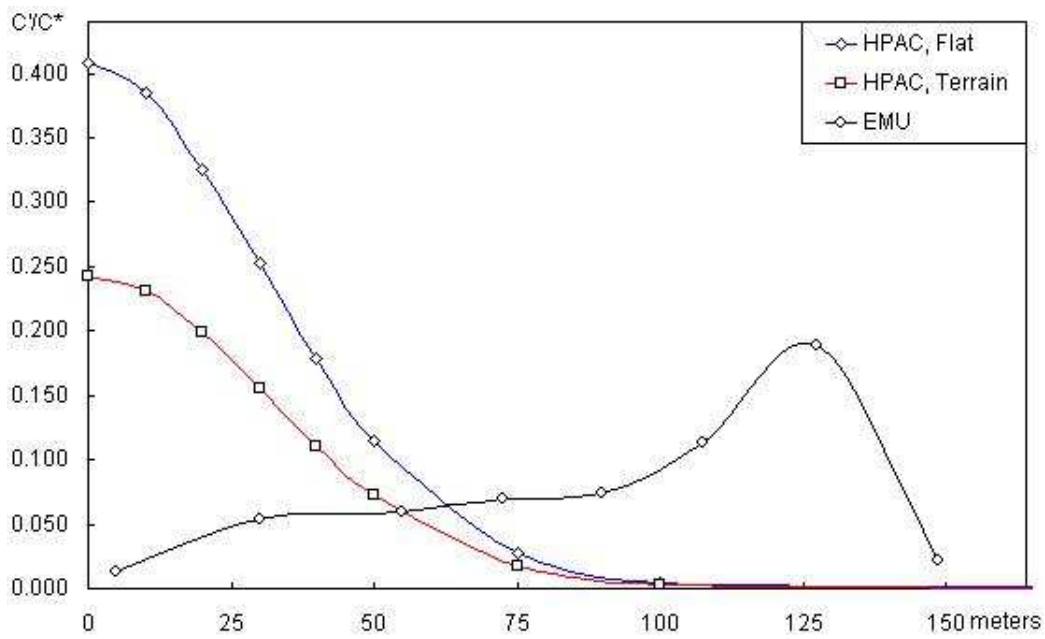


Figure 4.6: Cross-plume concentration profile at ground level, 110m downstream of the release. HPAC simulations compared to the experimental reference data.

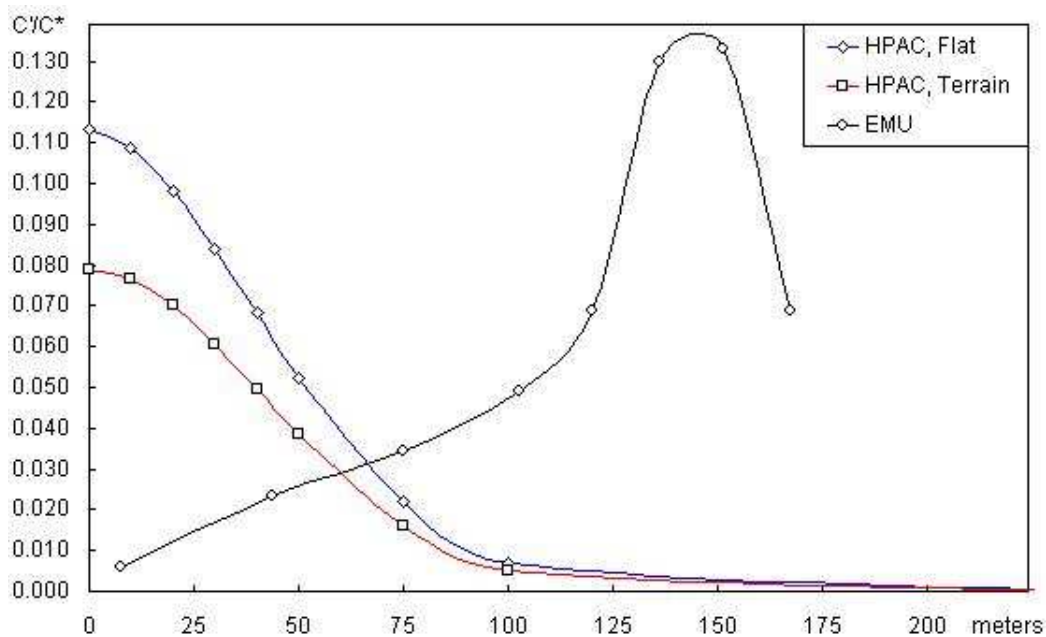


Figure 4.7: Cross-plume concentration profile at ground level, 195m downstream of the release. HPAC simulations compared to the experimental reference data.

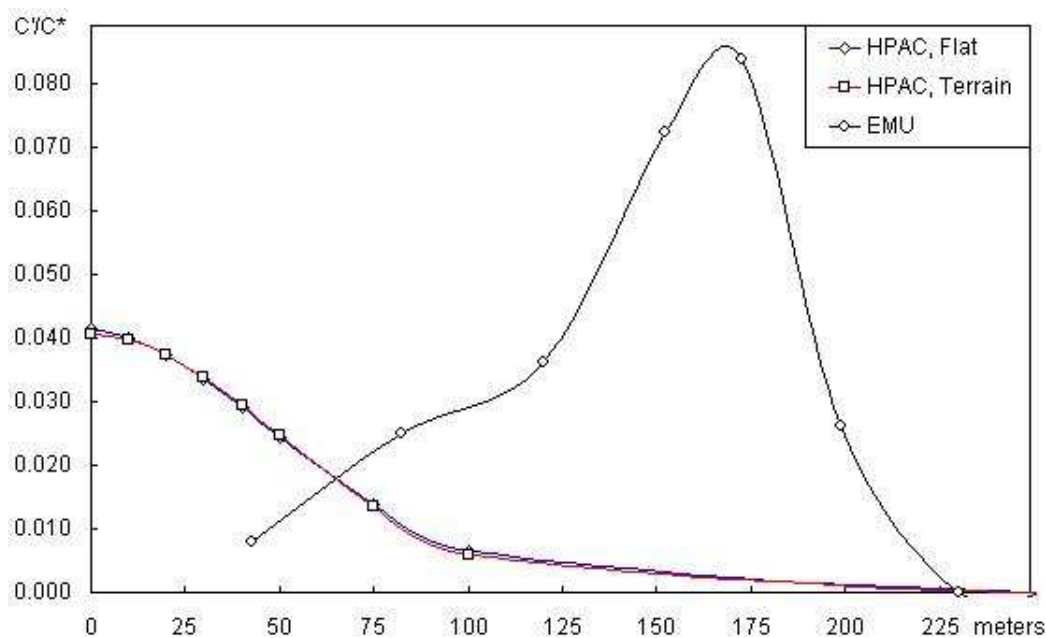


Figure 4.8: Cross-plume concentration profile at ground level, 300m downstream of the release. HPAC simulations compared to the experimental reference data.

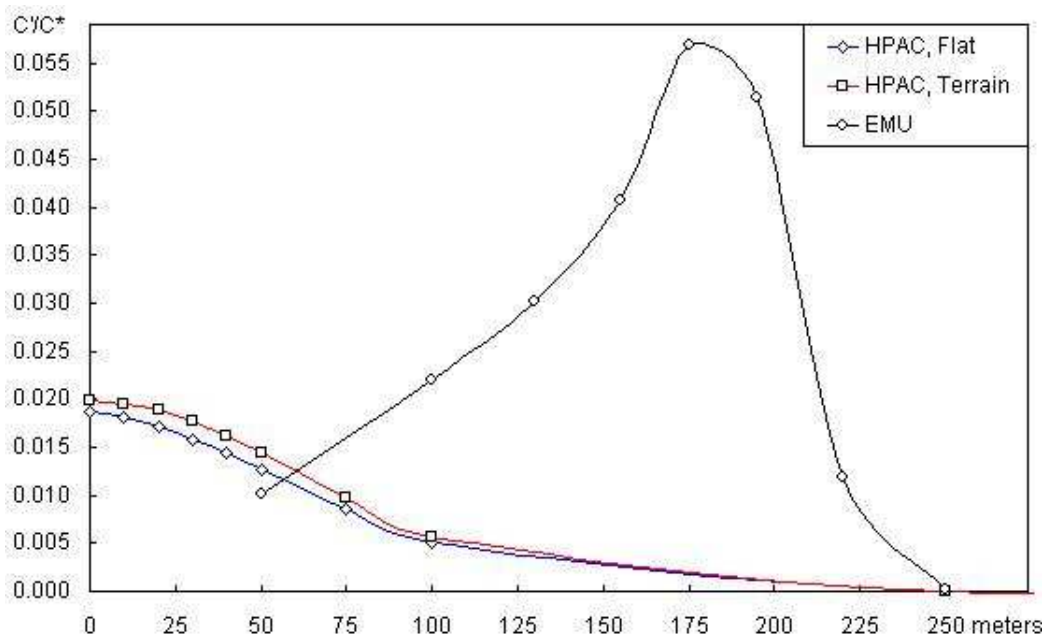


Figure 4.9: Cross-plume concentration profile at ground level, 450m downstream of the release. HPAC simulations compared to the experimental reference data.

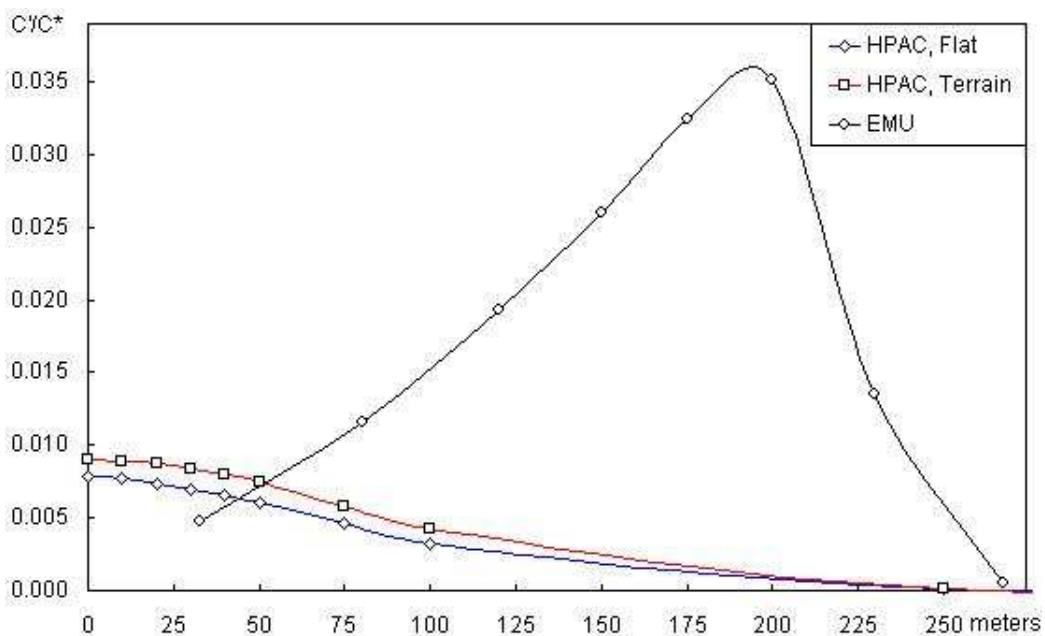


Figure 4.10: Cross-plume concentration profile at ground level, 675m downstream of the release. HPAC simulations compared to the experimental reference data.

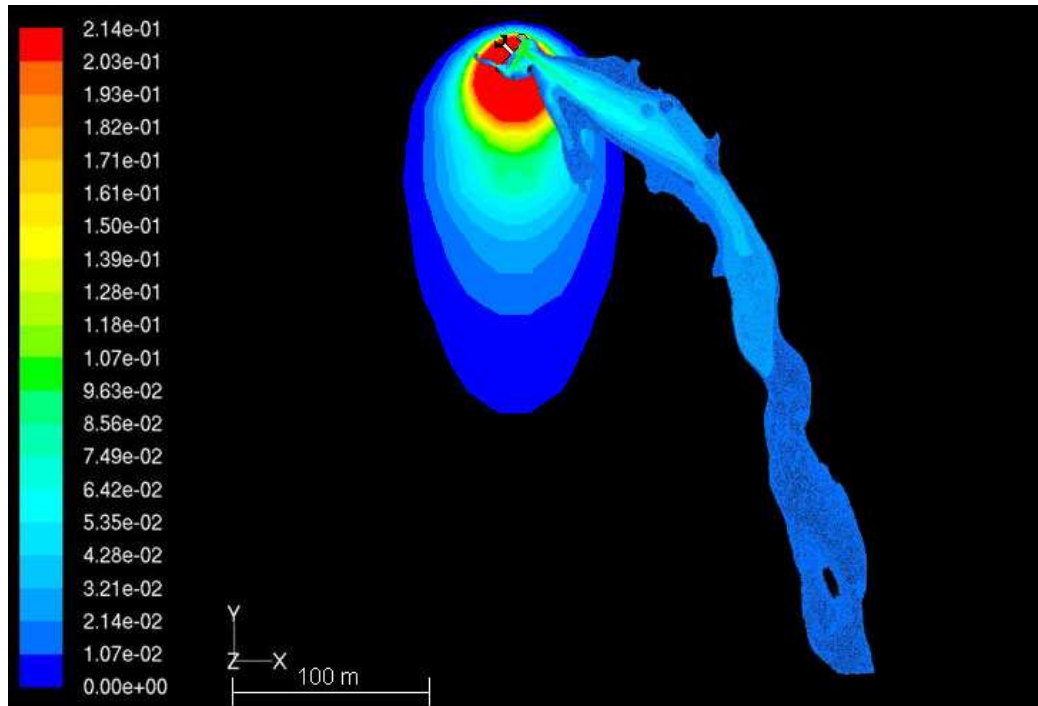


Figure 5.1: FLUENT and HPAC predictions of the chlorine gas plume at the end of the 900s release.

5 Conclusions

We have compared simulations using CFD techniques (FLUENT) and simple modeling (HPAC) against an experimental data set for the release and dispersion of Chlorine from an industrial facility. We compare the ground level footprint of the plumes for the two models in Fig. 5.1.

We find that CFD modeling can reproduce the reference data fairly well, both with respect to the trajectory of the plume and to the concentration values. The results do, however, show consistent under-prediction of the plume width and over-prediction of the peak concentration values.

HPAC simulations can not take into account deflection of the plume by the momentum-dominated release jet and plume-building interactions, and thus result in a plume aligned with the wind direction. Dilution of the plume appears to be more rapid in the simulations than in the reference. The plume is much wider in the near field than in the reference; this can in part be explained by the lack of a model to account for the momentum-driven jet release.

References

- [1] J. W. Bjerkelund. Analyse av utslipp og spredning av klogass ved bruk av FLUENT – en vurdering av modelloppbygning og beregning av spredning. MSc thesis, Department of Physics and Technology, University of Bergen., 2007.
- [2] J. W. Bjerkelund. Analyse av utslipp og spredning av klogass ved bruk av FLUENT – en vurdering av modelloppbygning og beregning av spredning. FFI/RAPPORT 2008/00302, Forsvarets Forskningsinstitut, 2008.
- [3] R.I. Sykes, D.S. Henn, S.F. Parker, and R.S. Gabruk. SCIPUFF - a generalized hazard dispersion model. Preprint of the 76th AMS Annual Meeting, Ninth Joint Conference on the Applications of Air Pollution Meteorology with A&WMA, 1996.
- [4] R.I. Sykes, C.P. Cerasoli, and D.S. Henn. The representation of dynamic flow effects in a Lagrangian puff dispersion model. *J. Haz. Mat. A*, 64:223–247, 1999.
- [5] I.R. Cowan and A.G. Robbins. Project EMU Experimental Data: Case C1. Technical report, EnFlo Research Centre, University of Surrey, 1996.
- [6] B. Carissimo, S. F. Jagger, N. C. Daish, A. Halford, S. Selmer-Olsen, K. Riikonen, J.M. Perroux, J. Wurtz, J. Bartzis, N. J. Duim, K. Ham, M. Schatzmann, and R. Hall. The SMEDIS database and validation exercise. *Int. J. Environment and Pollution*, 16:614–629, 2001.
- [7] S.F. Jagger, B. Carissimo, and N. Daish. Definition of parameters for model runs, WP4. Report SMEDIS/96/14/D, SMEDIS Project, October 1998. Draft, Version 0.5.